Eur. Phys. J. B **2**, 283–292 (1998)

THE EUROPEAN PHYSICAL JOURNAL B

Effect of changing microstructure of Y-Ba-Cu-O superconductors on the vortex motion under non-equilibrium thermal conditions

I. Kirschner[1,a], R. Laiho[2], A.C. Bódi[3], E. Lähderanta[2], and M. Marosvölgyi[4]

[1] Department for Low Temperature Physics, Eötvös University, 1088 Budapest, Hungary
[2] Wihuri Physical Laboratory, University of Turku, 20014 Turku, Finland
[3] Institute of Experimental Physics, Kossuth University, 4001 Debrecen, Hungary
[4] Department of Physics and Astronomy, University of Leiden, 2300 RA, Leiden, The Nederlands

Received: 17 December 1997 / Accepted: 28 January 1998

Abstract. Repetition of cooling and heating of high-T_c superconductors is detected to be able to result in some change of their microstructure. A non-equilibrium experimental technique provides direct measurement of the velocity of vortex motion in high-T_c Y-Ba-Cu-O superconductors. Its value falls in the interval of $8.3 \times 10^{-2} - 16.0 \times 10^{-2}$ mm/s depending on the number of the cooling or heating cycles, to which the samples are submitted. The thermal cycling created homogenization of the specimen's microstructure, and is presumed to cause this phenomenon, decreasing the number and strength of pinning centers. This supposition is proved by X-ray diffractography and transmission electron microscopy. A simple irreversible thermodynamic theory is elaborated to describe the reason, direction and dissipative character of the vortex motion.

PACS. 74.25.-q General properties; correlations between physical properties in normal and superconducting states – 74.40.+k Fluctuations (noise, chaos, nonequilibrium superconductivity, localization, etc.) – 74.60.Ge Flux pinning, flux creep, and flux-line lattice dynamics

Introduction

This paper is devoted to the systematic and quantitative study of how vortex motion in Y-Ba-Cu-O superconductors is affected by changing the microstructure of these materials. In order to realise the aim set, an earlier elaborated non-equilibrium procedure, the so-called thermometric mapping method (TMM) has been applied [1] to investigate the variation of the vortex motion caused by microstructural changes of Y-Ba-Cu-O samples. Experiments carried out show that the change in the material's microstructure can be directly produced by a series of cooling and heating processes to which the specimens were submitted. As has been experienced, the thermal cycling influences immediately the sample's microstructure inasmuch as it homogenizes the material, increasing its order. The material's ordering results in a decrease of the number of pinning centers, and of the strength of pinning forces, and so the vortices can move more easily in the samples. This effect manifests itself in faster vortex exchange between different local regions of specimens. Our experimental arrangement and procedure ensure suitable circumstances for the development of freer vortex motion, and they make possible the detection of the arising significant increase of the vortex velocity.

[a] Fax: 36-1-2660206.

Since all the other components of measuring conditions were fixed, the phenomenon observed can be attributed exclusively to the ordering effect of the thermal cycling. In this scenario, the series of cooling and heating processes can be taken into account as an additional and supplementary heat treatment of samples, leading to their final homogenization.

Whilst the presence of a temperature gradient represents a thermal force to promote the vortex motion, at the same time it broadens the normal superconducting (N−S) or superconducting normal (S−N) transitions, increases the time of their realisation, makes possible the observation of their fine structure [2], and distinguishes the local properties of the sample's material [3].

Experiments and results

The flow chart of this investigation can be drawn as follows:

1) measurement of the magnetic properties (mainly of the a.c. susceptibility) of the samples;
2) observation of the change of characteristic data during repeated measurements;
3) conclusions on the possible reason for the detected effect, which may be the thermal cycles;

4) control of this supposition by microstructural characterisation of specimens before and after an appropriately large number of cooling and heating processes;
5) comprehensive study of the correlation of the thermal cycling, microstructural changes and vortex motion;
6) determination of the dependence of the microstructure on the cooling and heating cycles, and that of the vortex motion on the change of the microstructure.

Samples were similar to those used in earlier experiments [4–6], having sizes of $6 \times 8 \times 12$ mm^3 and $6 \times 8 \times 22$ mm^3. They were prepared from fine Y(1,2,3) powder of sizes about 1 m by using a dynamic pressing method at high pressures according to the employment of the so-called mechano-chemical effect [7]. These specimens are very close to the single-phase material containing more than 95% $Y_1Ba_2Cu_3O_{7-\delta}$, other compounds such as $Y_1Ba_2Cu_4O_8$, Y_2O_3, $BaCuO_2$ and CuO less than 5%, and impurity elements such as Zn, V, Al, Ni, Cr, Si, Co, Fe and Ti not more than 0.005%. The preparation procedure mentioned above results in very compact samples of a density of 4.82−4.89 g/m^3 possessing very smooth surfaces. The latter feature has a significant importance in thermally non-equilibrium experiments, providing suitable touching contacts between metallic and ceramic elements of the measuring arrangement in order to regulate the temperature of the ends of specimens.

Determination of the temporal change of complex a.c. susceptibility χ provides reliable information on the vortex dynamics inside a given region and between different regions of the samples. Due to this reason, the investigation procedure can be formulated as the continuous and simultaneous measurement of the time-dependence of the real component χ' of χ of different macroscopic parts of the specimens, and that of the time-dependence of local temperatures at well-defined places of samples during cooling and heating processes. Each sample was covered by an excitation coil L_{exc} working at the frequency of $f = 100$ kHz and producing a low a.c. magnetic field in the order of $H_{a.c.} \sim 1$ G on the specimen's surface. Under this coil three independent and equivalent detection coils were closely wound on the top, middle and bottom parts of the samples. They possessed inductances L_t, L_m and L_b, respectively, depending on the actual state of the given part of specimen covered by them.

The above mentioned TMM is based on a wide and variable temperature gradient [8], to which the samples have to be submitted. To accomplish it simply [3], the top temperature T_t can be varied continuously with changing speed between room- and liquid nitrogen temperatures (or in another required temperature interval), while the bottom temperature T_b can be kept at liquid nitrogen ones. This procedure results in a variable temperature gradient along the sample. Application of a thermally insulating polyurethane foam coating prevents the intersecting heat flows. In this case the border line of normal and superconducting ranges passes slowly through the whole specimen along its axis according to the direction of the one-dimensional temperature gradient ∇T applied. The share-rate of normal and superconducting masses or volumes depends on local properties of samples in a given time moment at the actual local temperature and magnetic field. The resolution of the method is determined by the magnitude of ∇T, while the mapping velocity and sensitivity by the speed of the change of ∇T. Characteristic values of the existing temperature gradient were followed closely by four thermocouples placed on the bottom, between the pick-up coils and on the top of the specimens (see Fig. 1), detecting both the actual values of temperatures T_b, T_{mb}, T_{mt} and T_t, and their continuous temporal variation.

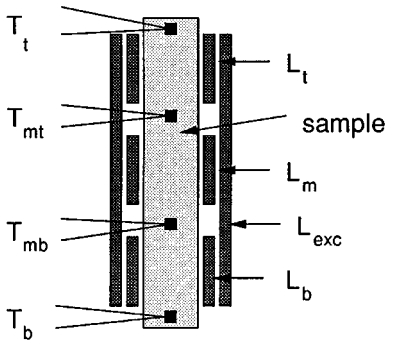

Fig. 1. Experimental arrangement of the measurement of a.c. susceptibility of different regions of the sample. The excitation coil L_{exc}, the detection coils L_b, L_m and L_t and the thermocouples T_b, T_{mb}, T_{mt} and T_t are placed on the specimen to detect the temporal change of magnetic properties and characteristic temperatures, respectively.

Since the amplitude of the a.c. magnetic field employed is low, it does not separate the intergrain and intragrain effects, and characterizes macroscopically the whole specimen, thus the change of the temperature in time during a cooling or heating stage reflects directly the local properties of the sample. The inductance of a detecting coil L_i depends on the number of vortex lines in the material encircled by the coil. This latter is determined by the actual value of the a.c. susceptibility χ', so the a.c. voltage signal U_i measured on the coil in question reflects the momentary state of co-existing normal and superconducting domains. The decreasing value of U_i represents an increasing superconducting and decreasing normal volume (or mass) fraction and *vice versa*. In this way, $U_i = \max$ corresponds to zero diamagnetism (*i.e.* zero superconducting material content) characterized by $L_i = \max$ and $\chi_i' = 0$, and so $U_i = 0$ to complete diamagnetism (*i.e.* total superconducting material content) marked by $L_i = 0$ and $\chi_i' = 1$ (in SI units). This scaling provides a simple method for the evolution of the measured data, because the changes of these parameters during a cooling or heating process play only a direct role in it. At the same time, the a.c. magnetic onset temperature T_0^m indicates the starting point in the scaling, since the inductances of the filled and empty coil are practically the same above this temperature.

On the basis of this consideration, the temporal change of U_t, U_m and U_b demonstrate, respectively, the temporal variation of characteristic L and χ', and together with them that of the superconducting and normal material

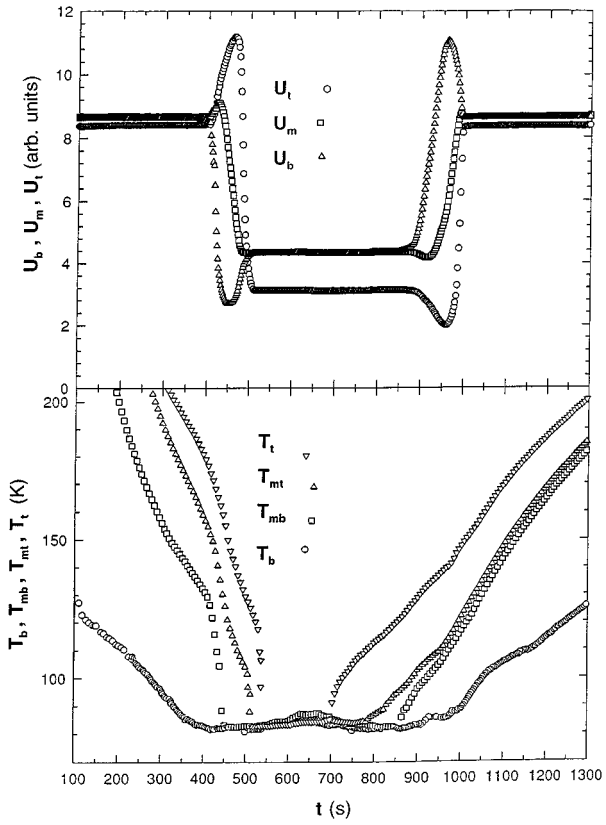

Fig. 2. Typical curves of a full thermal cycle, representing the variation of the magnetic susceptibility and temperature at different places of the sample.

(or volume) content which appeared due to the changing temperature gradient in the given sample's region.

During the execution of experiments, the specimen can be cooled with the help of a cold slab, the top end of which is in contact with the bottom of the sample and its opposite end is immersed into liquid nitrogen. To hasten the heating process of the top of the specimens either the application of a warm slab or use of a heating coil can be made.

Different experimental series were designed to be under computer control, collection of the measured temperature and inductance data utilised a Keithley DAS-TC acquisition card.

In order to detect the vortex motion between different regions of the specimen, the temperatures T_b, T_{mb}, T_{mt} and T_t at four points, and the a.c. voltage signals U_b, U_m and U_t of the pick-up coils have to be simultaneously measured as functions of the cooling and heating time t.

Typical curves of an entire thermal cycle are depicted in Figure 2, the upper part of which shows the dependence of the characteristic voltage signals on time, reflecting the actual values of L_i and χ_i' and the lower part that of the characteristic temperatures. Since the cooling of the sample begins at its bottom, the signal U_b decreases monotonically until the transition of the bottom region of the specimen, and after that increases to a limiting value. According to the physical facts reflected by this shape of the curve U_b *versus* t, the flux line density of the bottom region begins to decrease at the beginning of the cooling process. Later, attaining a minimum, it increases due to the interaction with the middle part of the sample, which just starts to cool, expelling its own flux lines. The exchange of the vortices between the bottom and middle regions, and so the equalization of their densities is the cause of the long-term common horizontal parts of the curves U_b and U_m. In contrast with the shape of U_b *versus* t, the curves U_m *versus* t and U_t *versus* t increase at first, reaching a maximum and after it they decrease. This type of curve characterizes the increasing, and after attaining a maximum value decreasing flux line densities, having some final limits, which develop in the middle and top regions due to the common effect of the cooling and flux exchange.

The shape of the a.c. voltage curves does not repeat itself in a fully symmetric way during the heating process. As the heating sets in at the top of the specimen, the increase of T_t and then T_{mt} calls forth the transition of the top region into the normal state, absorbing flux lines. The increase of the vortices in the top part augments the values of L_t and U_t, and reduces temporalily the values of L_m, U_m, L_b and U_b, demonstrating the transitional flux diffusion from the middle and bottom regions into the top one. The parallel non-linear temporal course of the initial heating sections of the curves T_{mt}, U_m, T_{mb}, U_b and T_b hints at the strong interaction between the magnetic and thermal phenomena, namely the mutual effect of local temperature variation and vortex dynamics on each other. This is the real reason for the significant non-linear behavior of both the curves $U_i{-}t$ and $T_i{-}t$. In the absence of thermodynamic cross-effects their increasing and decreasing section would be nearly linear.

As the consequence of the inhomogeneous and gradual cooling or heating of the specimens, which manifests itself in the existence of deviating local temperatures at a given time moment, a temporal delay can appear between the N−S or S−N transitions concerning different parts of the samples.

Comparing the branches of the curves U_i *versus* t corresponding to the cooling and heating stages, they show obviously a slight hysteretic character. During an earlier investigation [10] the nucleation of superconducting and normal domains was presumed as the reason of the hysteresis. This argument seems to be, however, questionable due to the experimental technique that regulates the velocity of the change of the temperature gradient applied on the samples, and together with this the number of normal and superconducting domains. In this way, based on a deeper analysis, the appearance of thermodynamic cross-effects, namely

1) the rise of thermo-electric power in the presence of normal and superconducting domains,
2) dissipative conversion of the thermal and magnetic energies into each other, resulting in local temperature increase or decrease,
3) thermal diffusion of the magnetic vortices and charge carriers and

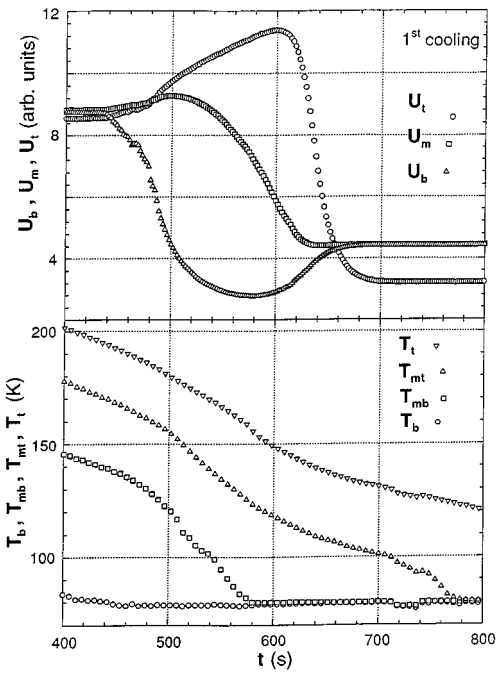

Fig. 3. Temporal change of the signals reflecting the actual magnetic state of different regions of the sample during the 1st cooling stage.

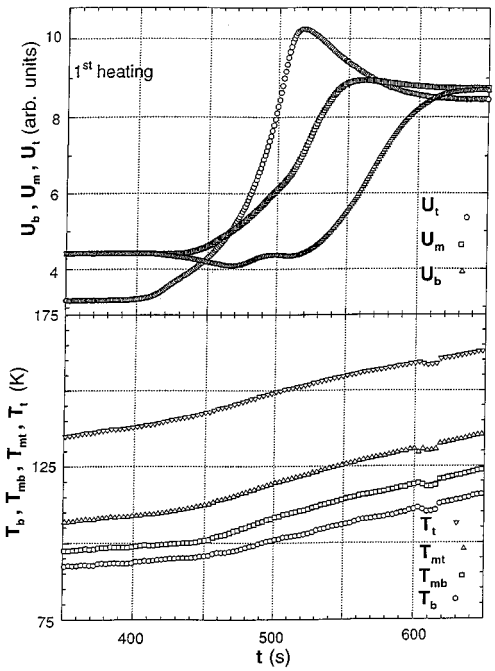

Fig. 4. Temporal change of the signals reflecting the actual magnetic state of different regions of the sample during the 1st heating stage.

4) change of the local vortex densities and velocities due to the inhomogeneous cooling and heating and the local thermal instabilities can be supposed to cause mainly the hysteretic feature of the curves characterizing the dynamic vortex state.

Setting out from the first qualitative observation the effect of thermal cycling on the vortex motion [9], we submitted systematically the samples to numerous cooling and heating processes and measured their a.c. susceptibility during them. The aim of this series of experiments was to find the essential components of the correlation between the increasing number of thermal cycles and the change of the motion of vortices, moreover to clear up the direct possible reason for the latter.

Analyzing the curves of Figure 3, characteristic to the first cooling process, a sharp decrease of U_b and a moderated increase of U_m and U_t are conspicuous, corresponding to decreasing L_b and increasing L_m and L_t, respectively. These shapes are formed by the starting repulsion of vortices from the bottom region of the sample, which flow partly into the middle and top regions. As the middle region becomes gradually superconducting, its vortices are expelled, streaming partially into the transitional top and superconducting bottom zones. In the course of the N−S transition of the upper region, the repulsed vortex lines increase the local magnetic field strength mostly in the lowest region and very little in the middle part of the sample, moreover in its close physical surroundings to a certain extent.

According to the heating characteristics of Figure 4, the S−N transition comes into being at first in the top range. It absorbs magnetic flux from the specimen's middle and bottom parts and its environments, too. This creates the first minimum of the curve U_b−t. During the gradual transition of the middle region into normal state, the vortices are absorbed from the upper and bottom regions of the sample, causing the second minimum of the curve U_b−t and a fast decrease of U_t. When the lowest region goes over into normal state, it calls forth the decrease of the local magnetic field intensity mainly in the top and very little in the middle regions, absorbing vortices from them.

As Figures 5−10 show, the situation is very similar during the thermal cycles of higher numbers, but the shape of curves become less sharp than in the first cooling or heating, and the time interval required for redistribution of the flux lines during N−S or S−N transition in the sample decreases significantly. Comparing the data of Figures 3−10 to each other, the systematic reduction of the time period needed for the equalization of the vortex distribution disturbed by cooling or heating seems to be inherent to the increasing number of thermal cycles. It was experienced that the velocity of the exchange of vortices between different regions of the specimen is influenced essentionally by its actual state. In the beginning of the measuring series the length of the time of the magnetic cycles decreases continuously with the increase of the number of thermal cycles. Then a saturation value sets in after reaching a sufficiently large number of cooling and heating cycles, and the speed of the vortex motion becomes constant.

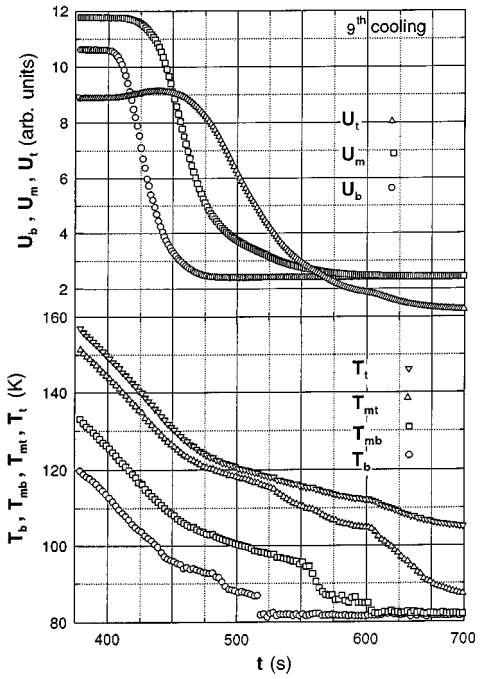

Fig. 5. Temporal change of the signals reflecting the actual magnetic state of different regions of the specimen during the 9th cooling stage.

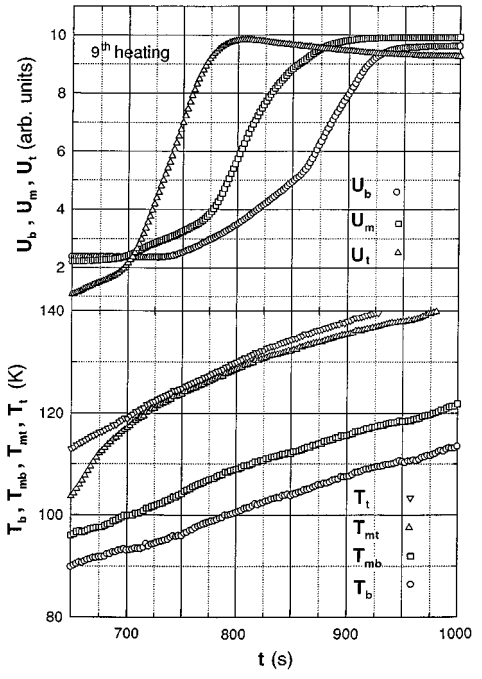

Fig. 6. Temporal change of the signals reflecting the actual magnetic state of different regions of the specimen during the 9th heating stage.

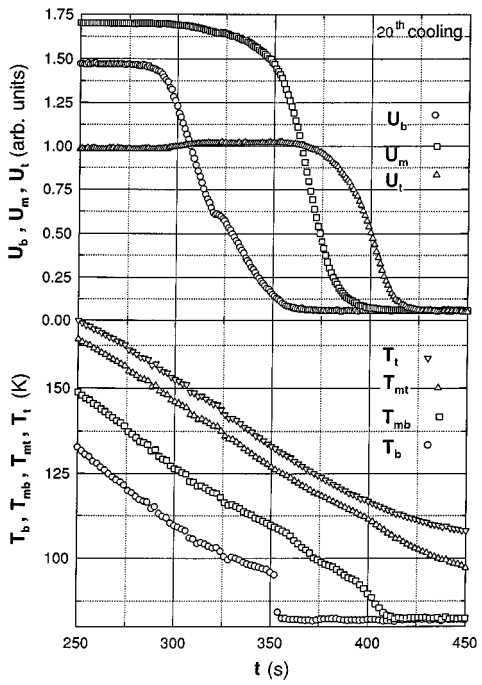

Fig. 7. Temporal change of the signals reflecting the actual magnetic state of different regions of the sample during the 20th cooling stage.

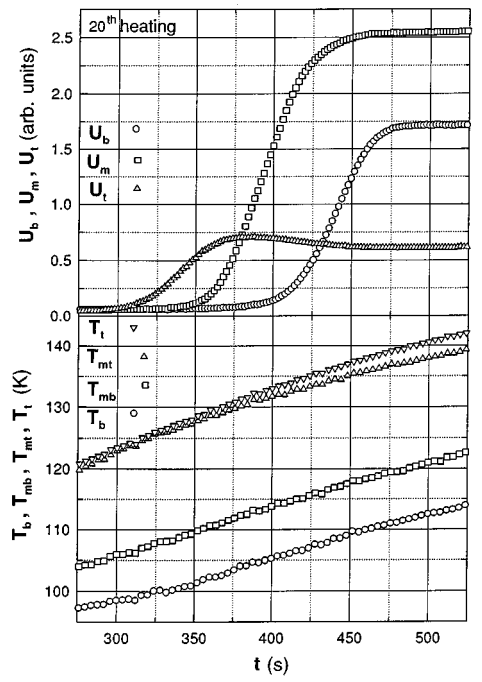

Fig. 8. Temporal change of the signals reflecting the actual magnetic state of different regions of the sample during the 20th heating stage.

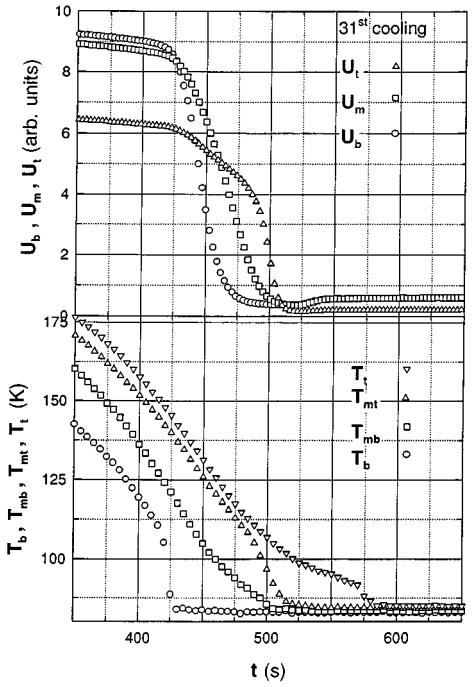

Fig. 9. Temporal change of the signals reflecting the actual magnetic state of different regions of the specimen during the 31st cooling stage.

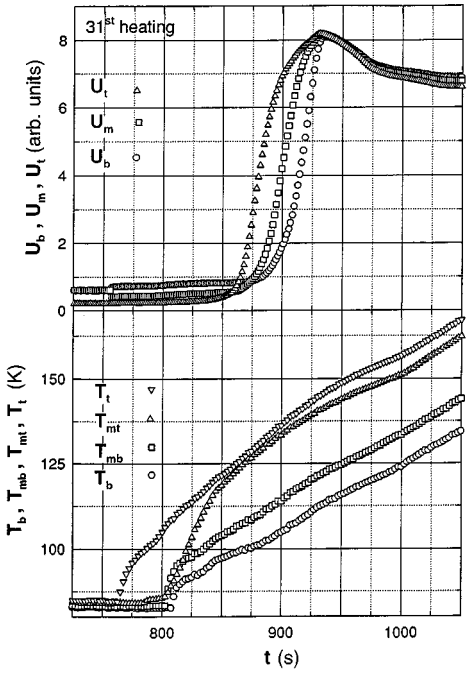

Fig. 10. Temporal change of the signals reflecting the actual magnetic state of different regions of the specimen during the 31st heating stage.

It is clear first of all that this non-equilibrium measuring method provides directly the values of the velocity of vortices in high-T_c superconductors and even its change during thermal cycles. Velocities related to the cooling and heating parts of the 1st, 9th, 20th and 31st cycle have the values of 8.7×10^{-2} mm/s and 8.3×10^{-2} mm/s, 12.5×10^{-2} mm/s and 10.2×10^{-2} mm/s, 15.4×10^{-2} mm/s and 13.3×10^{-2} mm/s, 16.0×10^{-2} mm/s and 14.8×10^{-2} mm/s, respectively.

This behavior of the vortex motion points out the dominant role of the number, size and strength of the pinning centers in the development of the vortex velocity. Under the unchanged experimental conditions the variation of the pinning properties is possible only, if the cooling and heating stages induce some change in the microstructure of the specimens and homogenize it, as a subsequent and additional heat treatment.

This statement has to be proved by structural investigation. This we performed by X-ray diffractography (XRD, Siemens D-5000) and transmission electron microscopy (TEM, Jeol 100 CXII) in selected area electron diffraction (SAED) and high resolution transmission electron microscopy (HREM) modes. The procedure consists of two independent series of measurements. The first of them was accomplished before the application of thermal cycles and the second after them, when finishing the earlier discussed experiments on the vortex motion.

XRD diffractograms show that the sample's material has well-crystallized $Y_1Ba_2Cu_3O_{7-\delta}$ of an essential quantity, in about 95%, supplemented by low quantity $Y_1Ba_2Cu_4O_8$ component and Y_2O_3, $BaCuO_2$ and CuO impurity compounds and some metallic elements in traces. The main deviation between the diffractograms before (Fig. 11) and after (Fig. 12) thermal cycling is in the full width at half maximums, which is bigger before, than after it. This property refers to the presence of a structural disorder, which decreases during the thermal cycles.

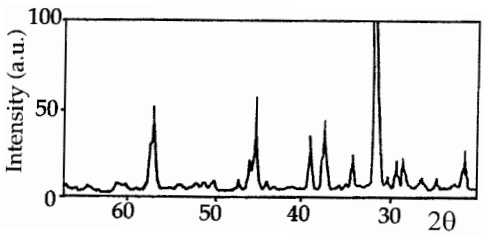

Fig. 11. X-ray diffractogram of the sample before thermal cycling, which has a larger full width at half maximum.

Without thermal cycling, the HRTEM micrographs demonstrate interstratification of $Y_1Ba_2Cu_3O_{7-\delta}$ and $Y_1Ba_2Cu_4O_8$ in (001)-planes corresponding to the thicknesses of 11.7 Å and 13.6 Å (see Fig. 13). This method also reveals the twinned character of the specimens, showing the presence of twin lamellae in (110)-planes (Fig. 14). As is seen in Figure 15, these disorders disappear during thermal cycling, which lead to highly homogeneous material. On the basis of these micrographs a higher, than conventional Cu-content can be presumed in the volume of structural errors, referring plausibly to the local presence of $Y_1Ba_2Cu_4O_8$ compound.

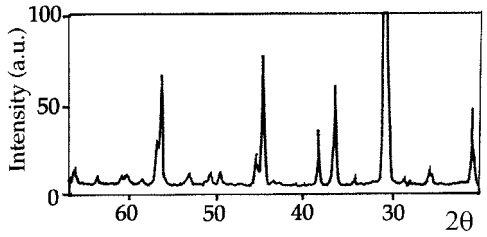

Fig. 12. X-ray diffractogram of the sample after thermal cycling, which has a smaller full width at half maximum, referring to the ordering of the sample's material.

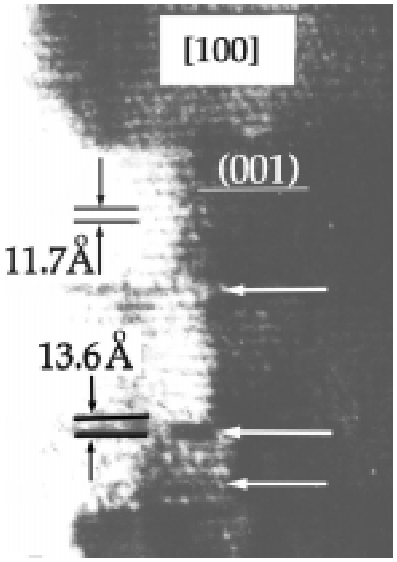

Fig. 13. A HRTEM micrograph which demonstrates the interstratification of $Y_1Ba_2Cu_3O_{7-\delta}$ and $Y_1Ba_2Cu_4O_8$ in the samples before the application of thermal cycles.

Similar results were given by SAED patterns as well, which show diffuse scattering of variable intensity in the c^*-direction, supporting the existence of random interstratifications (Fig. 16) in the specimens without thermal cycling, but they also cease (Fig. 17) during the employment of thermal cycles in the research of dynamic vortex properties.

In this manner, the structural investigation proves unambiguously that the change of the sample's microstructure is caused directly by the series of thermal cycles to which they were submitted during susceptibility measurements. On the basis of this observation the thermal cycles can really be explained as a subsequent heat treatment of specimens, that improves their homogeneity, decreases the number of pinning centers and the strength of pinning forces. This effect is responsible for the acceleration of the vortex motion during the increasing number of thermal cycles, as is discernible from Figures 3–10.

Comparison of the time intervals of the equalizing vortex motion belonging to different thermal cycles demonstrates not only the qualitative effect of thermal cycling, but provides the magnitude of the acceleration of the vortex motion, too. According to the experimental data of the Figures analyzed, the increase of the velocity of vortices was 84% concerning cooling and 78% concerning heating stages.

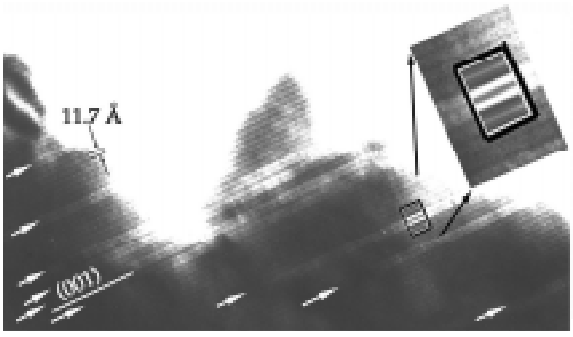

Fig. 14. A HRTEM micrograph showing twin lamellae in the specimens without thermal cycling.

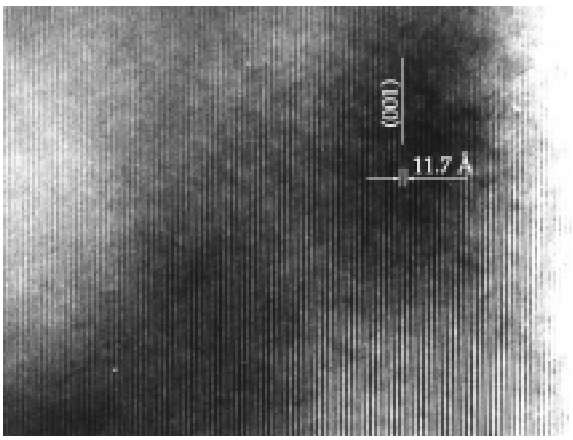

Fig. 15. A HRTEM micrograph, which demonstrates the disappearance of the disorder in the samples after thermal cycling.

As far as the fully homogenizing number of the thermal cycles is concerned, it depends strongly on the beginning state of a specimen's material, and generally falls between 20 and 30 in different measurement series performed.

Thermodynamic description of the vortex equalization process

The irreversible thermodynamics gives a framework for the investigation of macroscopic states and processes appearing in different solid states. A simple thermodynamic picture describes the reason, and prognoses the direction of the vortex motion, too. Disregarding other interactions in the first approximation, the change of the entropy ΔS in the course of the vortex motion between places (1) and (2) can be obtained as

$$\Delta S = -\left(\frac{\mu_v(1)}{T(1)} - \frac{\mu_v(2)}{T(2)}\right)\Delta N_v(1,\,2), \qquad (1)$$

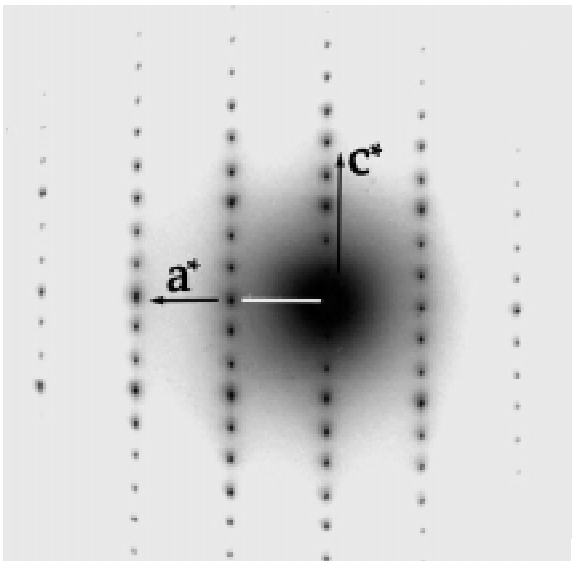

Fig. 16. The SAED pattern, having diffuse scattering, which represents random interstratification in the material before thermal cycling.

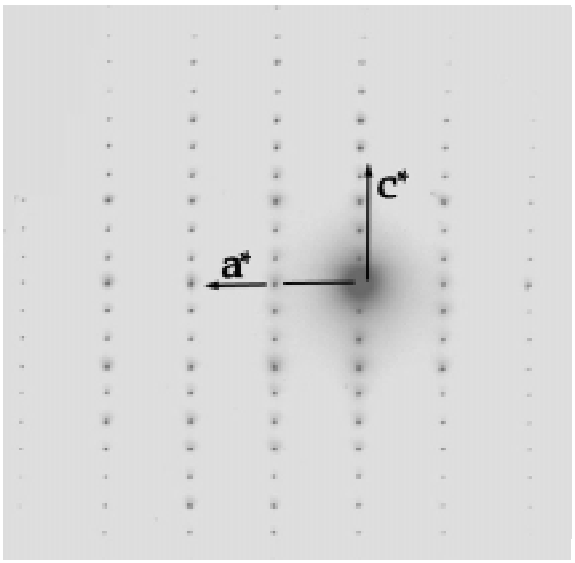

Fig. 17. The SAED pattern reflects the disappearance of the interstratification after the application thermal cycling. Figs.

where μ_v is the vortex chemical potential, T is the temperature and N_v is the quantity of vortices at the given places, respectively. According to the general thermodynamic requirement, by which ΔS has to be positive or at least zero ($\Delta S \geq 0$) during any equalization process,

$$\Delta N_v(2 \to 1) > 0, \quad \mu_v(2) > \mu_v(1)$$

if

$$\Delta N_v(1 \to 2) > 0, \quad \mu_v(1) > \mu_v(2), \tag{2}$$

supposing the equalization of the temperature is accomplished already along the sample. It means that vortices move always from the places having higher vortex chemical potential towards the places of lower vortex chemical potential. This statement points out the direction of the motion of the vortices. As far as the cause of vortex motion is concerned, this is the deviation of the values of the vortex chemical potential between different regions of the specimens. In compliance with it, the spatial inhomogeneity of μ_v represents a moving force for vortices. In this simplified case, only the distribution of the vortex chemical potential determines the motion of vortices.

If some other thermodynamic interactions, *e.g.* thermal and electrical ones are also taken into account, characterized by the temperature T, and electrical potential U, respectively, their difference (or gradient) will also play a role in establishing vortex dynamics. In this case the complex equation of the change of entropy ΔS will have the form

$$\begin{aligned}\Delta S = &\left(\frac{1}{T(1)} - \frac{1}{T(2)}\right) \Delta E(1,\,2) \\ &- \left(\frac{U(1)}{T(1)} - \frac{U(2)}{T(2)}\right) \Delta q(1,\,2) \\ &- \left(\frac{\mu_v(1)}{T(1)} - \frac{\mu_v(2)}{T(2)}\right) \Delta N_v(1,\,2) \geq 0, \end{aligned} \tag{3}$$

describing the reason and the direction of the vortex motion, where E is the internal energy and q is the electrical charge. Generalizing this consideration, it can be stated that all the inhomogeneities of intensive parameters existing in the sample at a given time moment contribute to the creation of the resultant force acting on the vortex lattice, which determines the motion of the vortices. As we applied a one-dimensional temperature inhomogeneity along the samples, it leads to three different consequences.

1) In the presence of normal and superconducting domains, ∇T has to induce a thermo-electric voltage and a power dissipation, that increases or decreases practically in one direction, causing the diffusion of flux lines.
2) The local heating and cooling [11,12] appearing during thermal cycles, changes the planar vortex distribution.
3) The effect of the thermal disturbance on the vortex motion, as a thermodynamic cross-interaction, must be observable, if all the other experimental conditions remain the same. The design of measurements to detect these secondary phenomena seems to be a prospective continuation of the research discussed.

On the other hand, the equalization of the intensive parameters forms a temporal decay of the force acting on the vortices to achieve an equilibrium state, developing meanwhile different thermodynamic cross-effects among

the thermal, electrical and magnetic interactions, which accelerate the equalization process as a dynamical Le Chatelier-Braun type principle.

The deviation from the equilibrium of a system can be described by macroscopic α-parameters, having a density or specific quantity character

$$\alpha_i = \frac{x_i - x_{i0}}{V}, \quad \text{or} \quad \alpha_i = \frac{x_i - x_{i0}}{N}, \tag{4}$$

where x_i is the actual, x_{i0} is the equilibrium value of the i-th extensive parameter, V is the volume and N is the mass expressed by the number of mols. In this scale the α-parameter of the entropy α_s can be determined as a function of the others:

$$\alpha_s = \alpha_s(\alpha_1, \alpha_2, ..., \alpha_n), \tag{5}$$

where n characterizes the number of possible interactions permitted by the isolations.

According to the method of irreversible thermodynamics, the forces X_i can be explained with the help of non-equilibrium deviations α_i of the extensive parameters in the form of homogeneous-linear relations

$$X_i = \sum_{k=1}^{n} -g_{ik}\alpha_k \quad i = 1, 2, ..., n, \tag{6}$$

where g_{ik} is the suitable element of the entropy matrix $\hat{g}$. As is seen, the non-equilibrium extensive deviations play a role in the constitution of the i-th force. Simultaneously, all of the thermodynamic forces (*i.e.* inhomogeneities of intensive parameters) develop together each current or flux density $j_i = \dot{\alpha}_i$ appearing in the given system. The relation between them can analytically be expressed by homogeneous-linear equations

$$\dot{\alpha}_i = \sum_{k=1}^{n} L_{ik}X_k \quad i = 1, 2, ..., n, \tag{7}$$

where L_{ik} is the proper element of the conductivity matrix $\hat{L}$. (It must be noted that both $\hat{g}$ and $\hat{L}$ are of the n-th order, quadratic, symmetric and positive-definite character).

Combination of the relations (6) and (7) results in the so-called thermodynamic equations of motion, having the matrix form of

$$\dot{\mathbf{X}}(t) = -\hat{g}\hat{L}\mathbf{X}(t) \tag{8}$$

and

$$\dot{\boldsymbol{\alpha}}(t) = -\hat{L}\hat{g}\boldsymbol{\alpha}(t), \tag{9}$$

which describe the actual equalization process after ceasing external disturbance, where t is the time. (Here the vectors $\mathbf{X}$ and $\boldsymbol{\alpha}$ mark all the possible forces and non-equilibrium deviations, respectively, existing in the system at a given time moment). The non-diagonal character of $\hat{g}$ and $\hat{L}$ ensures the existence of thermodynamic cross-effects. The solutions of (8) and (9) reflect the temporal decay of $X_i = X_i(t)$ and $\alpha_i = \alpha_i(t), i = 1, 2, ..., n$, since

$$\mathbf{X}(t) = \mathbf{X}_{initial}\, e^{-\hat{g}\hat{L}t} \tag{8'}$$

and

$$\boldsymbol{\alpha}(t) = \boldsymbol{\alpha}_{initial}\, e^{-\hat{L}\hat{g}t}. \tag{9'}$$

According to these relations, the state keeps to an equilibrium one, inasmuch as

$$\mathbf{X}(t) \to 0 \tag{8"}$$

and

$$\text{if } t \to \infty$$

$$\boldsymbol{\alpha}(t) \to 0 \tag{9"}$$

demonstrating the total equalization tendency in the undisturbed system.

In the case, when only the distribution of vortex potential is supposed to be inhomogeneous, the relation (7) provides the simplest possible conductivity equation for the vortex motion, including merely the thermodynamic force originated from the actual non-equilibrium behavior of this potential

$$\dot{\alpha}_v = j_v = L_v X_v, \tag{10}$$

where $X_v = \Delta\mu_v$ or $\nabla\mu_v$ and the vortex conductivity coefficient L_v can be calculated by thermodynamic method, as

$$L_v = T\frac{n_v\phi_0}{\eta_v}\,. \tag{11}$$

Here η_v is the conventional vortex viscosity factor, that is obtained from different experimental and theoretical results [13–15].

The dissipative character of the vortex motion can also be described in the framework of irreversible thermodynamics. The entropy production caused solely by the flux motion is given in the form

$$\sigma_v = \frac{1}{T}\eta_v v_v^2 n_v \phi_0 > 0, \tag{12}$$

which is the measure of the dissipation

$$D_v = T\sigma_v = \eta_v v_v^2 n_v \phi_0, \tag{13}$$

where v_v is the drift velocity of vortices and ϕ_0, is the magnetic flux quantum.

According to the equations (8') and (9'), the curves of the equalization reflect the exponential tendency of the temporal decay of the perturbation, except for the regions where the prominent role of thermodynamic cross-effects and strong flux exchange cause a significant deviation from it, but finally the decay of the perturbation will be exponential.

Recently a large, phase-periodic oscillation of the resistance (or conductance) of an N/S interface was observed [16]. The sample consists of a diffusive normal metal (Ag) and a superconducting metal (Pb), working in the mesoscopic range, at the presence of coexisting normal and superconducting materials at liquid helium temperatures. The oscillation was found to be highly sensitive to the variation of the temperature, controlling current and external magnetic field. This phenomenon provides an independent proof for the existence of cross-effects in superconductors among electrical, thermal and magnetic interactions and can generally be explained in the frame of irreversible thermodynamics. From this point of view it can be treated as a similar phenomenon to our measurements, where thermomagnetic cross-effects influence the shape of characteristic curves.

Conclusions

The investigations discussed above lead to some conclusions which can be summarised as:

1) Application of the thermometric mapping method (a large and variable temperature gradient together with the measurement of the a.c. susceptibility) is able to detect the fine structure of normal superconducting or superconducting normal transition, local and transient peculiarities of the vortex dynamics and to localize them by using spatially distributed measuring coils. During conventional isothermic experiments these fine and secondary phenomena are covered by the spatially and temporally averaged response of the samples.
2) Observation of perturbation effects induced by the interaction between the non-equilibrium thermal condition and the vortex motion in the form of unstable, fluctuating local heating and cooling, contributes to a deeper description of N−S and S−N phase transitions of high-T_c superconductors.
3) The method is sensitive enough to clear up immediately the effect of the cooling and heating process on the vortex dynamics and to determine the chain of correlations between thermal cycling, microstructure, and dynamic vortex properties. The present series of investigation explored the thermal cycles to be able to homogenize Y-Ba-Cu-O high-T_c superconducting materials, to decrease the number and strength of pinning centers, thus to promote the motion of flux lines, increasing substantionally their velocity. Although the research analyzed above provides useful qualitative and quantitative information on this problem, to reach an unambiguous and detailed connection between the thermal cycling, induced microstructural change, and the vortex motion requires numerous further experiments. They must be carried out on different kinds of samples in the presence of different magnetic fields and temperature gradients. Among others, those measurements may support or reject the first observation on the possible difference of the velocity increase between the cooling and heating processes and in the first case clear up its reason.
4) This investigation can also be continued in the direction to detect experimentally the role of thermodynamic cross effects in the vortex motion providing, at the same time, results for controlling the scope of irreversible thermodynamics in the field of high-T_c superconductors.

References

1. I. Kirschner, A.C. Bódi, R. Laiho, E. Lähderanta, Physica C **252**, 22 (1995).
2. I. Kirschner, S. Leppävuori, A.C. Bódi, A. Uusimäki, I. Dódony, Appl. Supercond. **1**, 1721 (1993).
3. I. Kirschner, R. Laiho, A.C. Bódi, E. Lähderanta, Physica C **290**, 206 (1997).
4. A.C. Bódi, I. Kirschner, S. Leppävuori, Z. Phys. B **97**, 481 (1995).
5. I. Kirschner, A.C. Bódi, R. Laiho, E. Lähderanta, Superlatt. Microstruct. **21**, 315 (1997).
6. I. Kirschner, A.C. Bódi, S. Leppävuori, A. Uusimäki, J. Dódony, T. Porjesz, Phys. Lett. A **178**, 315 (1993).
7. A.C. Bódi, I. Kirschner, R. Laiho, E. Lähderanta, Solid State Commun. **98**, 1049 (1996).
8. A.C. Bódi, I. Kirschner, S. Leppävuori, Phys. Lett. A **158**, 318 (1991).
9. I. Kirschner, A.C. Bódi, R. Laiho, E. Lähderanta, J. Mater. Res. **12**, N° 11 (1997).
10. A.C. Bódi, R. Laiho, I. Kirschner, E. Lähderanta, Z. Phys. B **104**, 33 (1997).
11. M. Frank, A. Singsaas, Z. Stodolsky, S. Cooper, Phys. Rev. B **43**, 5321 (1991).
12. I. Kirschner, K. Martinás, J. Low Temp. Phys. **14**, 427 (1974).
13. Y.B. Kim, C.F. Hempstead, A.R. Strnad, Phys. Rev. Lett. **13**, 794 (1964).
14. M. Yu. Kuprianov, K.K. Likharjev, Pis'ma v JETP **15**, 349 (1972).
15. E.H. Brandt, Act. Pass. Electr. Comp. **15**, 193 (1993).
16. V.T. Petrashov, R. Sh. Shaikhadarov, I.A. Sosnyin, Pis'ma v JETP **64**, 789 (1996).